Chemical Engineering Journal 155 (2009) 442–450

Contents lists available at ScienceDirect

Chemical Engineering Journal

journal homepage: www.elsevier.com/locate/cej

Direct synthesis of mesoporous M-SBA-15 (M = Al, Fe, B, Cr) and application to 1-hexene oligomerization

R. van Grieken*, J.M. Escola, J. Moreno, R. Rodríguez

Department of Chemical and Environmental Technology, ESCET, Universidad Rey Juan Carlos, C/Tulipán s/n, 28933 Móstoles, Madrid, Spain

ARTICLE INFO

Article history:
Received 3 April 2009
Received in revised form 26 June 2009
Accepted 2 July 2009

Keywords:
1-Hexene
Oligomerization
Direct synthesis
SBA-15
Acid catalysts

ABSTRACT

M-SBA-15 materials (M = Al, B, Cr, Fe) were prepared by different direct synthesis methods, characterized and tested catalytically in the 1-hexene oligomerization reaction at 125 °C. Al-SBA-15 were synthesized within the range Si/Al = 12–86 using aluminium isopropoxide as aluminium source. ^{27}Al MAS NMR spectra point out that the three Al-SBA-15 samples contain more tetrahedral aluminium than octahedral and the ratio tetrahedral/octahedral diminished with increasing aluminium contents. B-SBA-15 was prepared with a Si/B = 51–106 using two direct synthesis methods (sol–gel and hydrothermal) and three different boron sources (solid boric acid, aqueous boric acid and boron isopropoxide). The best results in terms of boron incorporation (Si/B = 51) were achieved with solid boric acid and the sol–gel method, although a lower degree of mesoscopic ordering was obtained compared to the hydrothermal procedure. ^{11}B MAS NMR showed that trigonal boron is the principal coordination state obtained after calcination. Cr-SBA-15 was also achieved by direct synthesis method at different pH (1.5, 3, 5) but the incorporation degree was low, at best Si/Cr = 240 at pH 5. UV–vis spectroscopy indicated that all Cr species were Cr^{6+} formed during the calcination step. Oligomerization of 1-hexene at 125 °C showed that the highest conversion (~30%) was attained over Al-SBA-15 (Si/Al = 30) although Cr-SBA-15 material exhibited close conversion (21%) despite its low heteroatom content (Si/Cr = 240). Dimers were the major products over Al-SBA-15, Cr-SBA-15 and Fe-SBA-15 catalysts (selectivity ≥ 40%) while strikingly, sol–gel B-SBA-15 lead mostly to heavy oligomers (>60%), with less than 10% of dimers.

1. Introduction

The oligomerization of light olefins ($C_3^=$–$C_6^=$) over acid catalysts is an interesting alternative for the production of higher molecular weight hydrocarbon mixtures useful as fuels (e.g. gasoline, diesel) and lubricants [1]. Both Brönsted and Lewis acids have been used as oligomerization catalysts in either homogeneous (H_2SO_4, organometallic complexes, etc.) or heterogeneous (mixed oxides, zeolites, clays, etc.) phases [2]. One of the most successful oligomerization processes is the MOGD ("Mobil Olefin towards Gasoline and Distillate") which allows preparing either gasoline (C_5–C_{12}) or diesel (C_{13}–C_{22}) by chosing properly the operation variables (T = 200–300 °C, P = 1–5 MPa, WHSV = 0.1–0.5 h^{-1}), employing microporous HZSM-5 zeolite as catalyst [3–6]. HZSM-5 is a 10-membered ring zeolite (MFI topology) with two types of microporous channels (0.51 nm × 0.55 nm; 0.54 nm × 0.56 nm) and strong acidity. The shape selectivity properties of the HZSM-5 enables even to obtain nearly linear hydrocarbons when the external acid sites are poisoned with 2,6-di-tert-butylpyridine, as the oligomerization reactions proceed only inside the micropores [7].

Liquid oligomerization of light alkenes ($C_4^=$–$C_6^=$) towards gasoline and diesel could become a way to use these olefins considered as by-products of the fluid catalytic crackers streams (FCC), attaining the formation of more valuable hydrocarbons. The catalyst plays a key role determining both activity and selectivity in the process, whereas the presence of solvents (n-octane, dodecane) slowed down catalyst deactivation [8]. Different catalysts have been tested: zeolites (HZSM-22, Al-TS-1, HZSM-57) [9–11], zeotypes (SAPO-11) [12], amorphous silica–alumina [13], small crystal size zeolites [14–16] and mesostructured materials (Al-MCM-41, Al-MTS, Al-SBA-15) [16–19]. The best results were obtained over mesoporous Al-MCM-41, Al-MTS, Al-SBA-15 and nanozeolites (HBeta, n-HZSM-5) since the presence of micropores was shown to be detrimental [14]. Thus, the selectivity towards oligomers (dimers + trimers) was higher than 70% at conversion values above 80%. In addition, mesoporous Al-MTS and Al-MCM-41 exhibited practically no deactivation in the 1-hexene oligomerization under the presence of nitrogen and sulphur poisons (n-butylamine and thiophene, respectively) [20].

Besides aluminium, other heteroatoms may be incorporated into the framework of the mesostructured material in order to pro-

* Corresponding author. Tel.: +34 91 488 70 07; fax: +34 91 488 70 68.
E-mail address: rafael.vangrieken@urjc.es (R. van Grieken).

1385-8947/$ – see front matter © 2009 Elsevier B.V. All rights reserved.
doi:10.1016/j.cej.2009.07.016

vide the oligomerization catalytic sites (acid, coordinating sites) with different activity and selectivity. So, Cr/H-MCM-41 gave rise mostly to heavy oil in the 1-hexene oligomerization (56% > C30) [21] while B-HZSM-5 yielded a high selectivity to tetramers in 1-butene oligomerization [22]. Therefore, the synthesis of mesostructured materials with different heteroatoms (Cr, B, etc.) appears to be an aim of utmost interest in the field of olefin oligomerization. The preparation of heteroatom-containing SBA-15 materials is particularly difficult due to the strong acid conditions required in the synthesis of this mesoporous solid. Under such conditions, a lot of elements exist only in the cationic form and they are hardly introduced in the mesostructure via condensation process with silicon species [23]. However, some authors have reported successful direct methods to incorporate different heteroatom into SBA-15 structure. So, Yue et al. [24] presented a successful direct method to prepare Al- SBA-15 with low Si/Al ratios (10 and 20) by an hydrothermal procedure at pH 1.5 using aluminium tri-tert-butoxide as a precursor. A similar direct route was used by Dragoi et al. [25] but using aluminium isopropoxide as aluminium source. Wang and Liu [26] developed a method to prepare Al-SBA-15 materials with Si/Al atomic ratios from 10 to 100 via evaporation-induced self-assembly process. Aguado et al. [27] combined the incorporation of aluminium and chromium on SBA-15 structure (Si/Al = 35 and Si/Cr = 66) by a direct route using aluminium isopropoxide and chromium nitrate at different pH values (0–3). Chromium species were also incorporated in the framework of SBA-15 by Selvaraj and Kawi [28] by using NH_4F acidic and pH-adjusting methods. A similar method was used by the same authors in order to synthesize Ga-SBA-15 materials from different Ga sources [29]. Melero et al. prepared Ti-SBA-15 catalysts in one step under strong acidic conditions starting from titanocene dichloride with Si/Ti ratios in the range 13–40 [30]. Newalkar et al. synthesized Ti-SBA-15 (Si/Ti = 5–40) and Zr-SBA-15 (Si/Zr = 20–80) mesoporous materials by means of a direct method under micro-wave-hydrothermal conditions [31]. Martínez et al. [32] reported the preparation of Fe-SBA-15 materials by a direct displacement of the template with ethanolic solutions containing Fe species whereas Vinu et al. [33] achieved the direct synthesis of iron-substituted SBA-15 materials with various Si/Fe ratios by adjusting the pH of gel mixtures above the isoelectric point of silica. As can be observed, "pH adjusting" methods have been used by several authors to achieve metal ions highly substituted into mesoporous SBA-15 walls [28,29,34]. In conclusion, according to the literature pH control and type of metal precursor are the main variables to obtain highly ordered mesoporous materials and a high metal incorporation degree.

In this paper, we report the direct synthesis and characterization of M-SBA-15 materials where M is aluminium, iron, boron or chromium. Different synthesis procedures (sol–gel and hydrothermal), pH values (0–5) and Si/M molar ratios were used. The obtained catalysts were tested in the 1-hexene oligomerization reaction in order to determine their catalytic properties in terms of both activity and selectivity.

2. Experimental

2.1. Synthesis of the catalysts

2.1.1. Al-SBA-15 materials

Al-SBA-15 materials were prepared according to the direct synthesis procedure reported by Yue et al. [24] but using aluminium isopropoxide as aluminium source and working with Si/Al molar ratios equal to 10, 30 and 60. In a typical synthesis, 8.6 g of tetraethylorthosilicate (TEOS, 98 wt.%, Aldrich) and a calculated amount of aluminium isopropoxide (AIP, Aldrich) for obtaining the desired Si/Al ratio, were added to 10 ml of aqueous HCl at pH 1.5. This mixture was stirred for 4 h at room temperature and then added to a second solution containing 4 g of Pluronic 123 in 150 ml of aqueous HCl at pH 1.5. Afterwards, the solution was stirred for 20 h at 40 °C and aged at 110 °C for 24 h under static conditions. The solid product was recovered by filtration, dried at room temperature overnight and calcined at 500 °C for 5 h using a heating rate of 0.4 °C min^{-1}.

2.1.2. Fe-SBA-15 materials

The preparation of these materials was carried out according to the procedure described by Martinez et al. [32]. In a typical synthesis, 4 g of Pluronic 123 was dissolved under stirring in 125 ml of 1.9 M HCl at room temperature. The solution was heated up to 40 °C before adding the iron precursor ($FeCl_3 \cdot 6H_2O$, Aldrich) dissolved in 1.9 M HCl. This mixture was maintained at 40 °C during 30 min and subsequently, 8.6 g of TEOS was added. The Si/Fe molar ratio in the synthesis gel was fixed at 30. The resultant solution was stirred for 20 h at 40 °C, followed by aging at 110 °C for 24 h under static conditions. The solid product was recovered by filtration and dried at room temperature overnight. The template was removed from the as-made mesoporous material by calcination at 550 °C for 5 h using a heating rate of 1.8 °C min^{-1}.

2.1.3. B-SBA-15 materials

B-SBA-15 materials were prepared according to two different procedures: sol–gel and hydrothermal. Three different compounds were used as boron sources: boron isopropoxide (+98 wt.%, Aldrich), boric acid aqueous solution (4 wt.%, Aldrich) and solid boric acid (Aldrich).

(a) Sol–gel method. 4 g of Pluronic 123 was dissolved under stirring in 125 ml of 1.9 M HCl at room temperature. The solution was heated up to 40 °C before adding the boron source and maintaining at 40 °C during 30 min. Thus, 8.6 g of TEOS was added obtaining a Si/B molar ratio in the synthesis gel equal to 30. The resultant solution was stirred for 75 min. Then, condensation reactions were promoted by dropwise addition of a 2 wt.% aqueous ammonia solution up to pH 4 and then, the stirring was hold for 1 h. The solid product was recovered by filtration and dried at room temperature overnight. The template was removed by calcination at 550 °C for 5 h with a heating rate of 1.8 °C min^{-1}.
(b) Hydrothermal method: this procedure is identical to the previously described for the synthesis of Fe-SBA-15 but using the aforementioned boron precursors.

2.1.4. Cr-SBA-15 materials

These materials were prepared by a procedure very similar to the previously described for the synthesis of Al-SBA-15 materials but varying the pH in the range 1.5–5. In this case, the heteroatom precursor was chromium nitrate ($CrNO_3 \cdot 9H_2O$, Aldrich) and the Si/Cr molar ratio in the synthesis gel was 30. In a typical synthesis, 8.6 g of tetraethylorthosilicate (TEOS, Aldrich) and 0.55 g of $Cr(NO_3)_3 \cdot 9H_2O$ (Si/Cr = 30), were added to 10 ml of aqueous HCl at the selected pH value (1.5, 3 or 5). This mixture was stirred for 4 h at room temperature and then added to a second solution containing 4 g of Pluronic 123 in 150 ml of aqueous HCl at the same pH than the first solution. The resultant mixture was stirred for 20 h at 40 °C, followed by aging at 110 °C for 24 h under static conditions. The solid product was recovered by filtration, dried at room temperature overnight and calcined at 550 °C for 5 h (heating rate = 1.8 °C min^{-1}).

2.2. Catalysts characterization

X-ray powder diffraction (XRD) patterns were acquired on a Philips X'PERT MPD diffractometer using Cu Kα radiation. XRD patterns within the $2\theta \sim 0.5$–10° range were obtained using

a step size of 0.02° and a counting time of 10 s. Nitrogen adsorption–desorption isotherms at 77 K were obtained with a Micromeritics Tristar 3000 apparatus. The samples were previously out-gassed under vacuum at 250 °C for 4 h. Surface areas were calculated with BET equation whereas pore size distributions were determined by the BJH method applied to the adsorption branch of the isotherms. Mean pore size was obtained from the maximum of BJH pore size distribution. Pore volumes were determined from the nitrogen adsorbed volume at $P/P_0 = 0.95$. Transmission electron micrographs (TEM) were collected on a Phillips TECNAI 20 microscope equipped with a LaB_6 filament under an accelerating voltage of 200 kV. Prior to the observation, the samples were dispersed in acetone, stirred in an ultrasonic bath and finally deposited over a carbon-coated copper grid.

Chemical composition of the M-SBA-15 materials was measured by ICP-atomic emission spectroscopy on a Varian Vista AX Axial CCD Simultaneous ICP-AES spectrometer. Previously, the sample was digested by acid treatment with H_2SO_4 and HF. The acid properties of the catalysts were determined by ammonia temperature programmed desorption (TPD) in a Micromeritics AutoChem 2910 system using He as carrier gas. The physisorbed ammonia was removed by flowing helium at 180 °C for 90 min. The chemisorbed ammonia was determined by increasing the temperature with a heating rate of 15 °C min^{-1} up to 550 °C. The ammonia concentration in the effluent helium stream was measured with a calibrated thermal conductivity detector (TCD). Solid state ^{27}Al and ^{11}B magic angle spinning nuclear magnetic resonance spectra (^{27}Al MAS–NMR and ^{11}B MAS–NMR) were recorded at 104.26 and 128.30 MHz, respectively in a Varian Infinity 400 instrument. The sample spinning rate was 11 kHz for ^{27}Al MAS–NMR and ^{11}B MAS–NMR. For ^{27}Al MAS–NMR, 2.5 μs pulses were used and 4000 free induction decays were accumulated with a repetition time of 3 s. For ^{11}B MAS–NMR, 0.5 μs pulses were used and 20,000 free induction decays were accumulated with 5 s repetition time. These measurements were carried out at room temperature using $Al(H_2O)_6^{+3}$ or H_3BO_4 (0.3 M) as external standard references. Diffuse reflectance Uv–vis spectra (DRS) of the as-synthesized and calcined Cr-SBA-15 materials were obtained under ambient conditions on a CARY-1 spectrophotometer equipped with a diffuse reflectance accessory in the wavelength range of 300–700 nm. A halon white reflectance standard was used as a reference material.

2.3. Oligomerization of 1-hexene

In the 1-hexene oligomerization reactions 1.5 g of catalyst and 20 ml of reaction mixture were loaded in a round bottom flask hold at 125 °C under stirring and reflux during 6 h. The composition of the reaction mixture was: 30 wt.% of 1-hexene (98 wt.%, Aldrich), 65 wt.% of n-octane (solvent, 99 wt.%, Aldrich) and 5 wt.% of n-heptane (internal standard, 99 wt.%, Aldrich). After the reaction, the flask content was cooled down to room temperature, the catalyst was removed by filtration and the oligomerization products were analyzed.

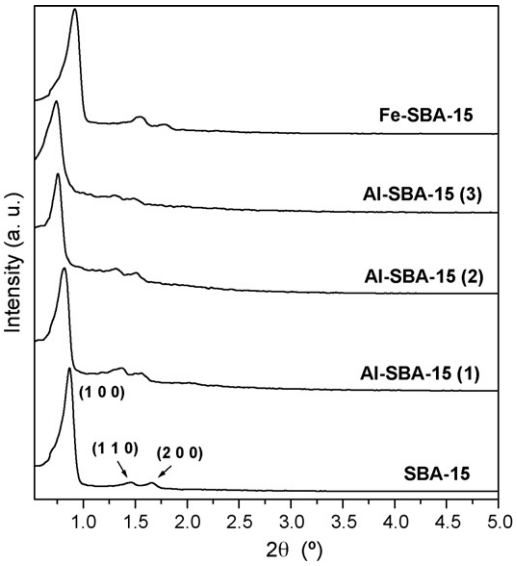

Fig. 1. XRD patterns of calcined Al-SBA-15, Fe-SBA-15 and pure-siliceous SBA-15 materials.

2.4. Analysis of the oligomerization products

The analysis of the as-obtained liquid and gaseous products was carried out by gas chromatography (GC) in a 3900 Varian GC equipped with a flame ionization detector (FID) and a 15 m length × 0.25 mm width CP SIL-8CB capillary column. The products were classified into several groups based on their respective GC retention times with regards to pure n-paraffin calibration standards. Both 1-hexene and all its isomers (e.g. 2-hexene, 3-hexenes, etc.) were lumped together as "hexenes" for the calculations. Hence, the conversion $X_{hexenes}$ was defined as (mass of converted hexenes) (mass of 1-hexene initially loaded)$^{-1}$ × 100. Selectivity was calculated as (mass of product fraction) (mass of reacted hexenes)$^{-1}$ × 100. The following fractions were defined for the selectivity calculations: S_{crack} (light C_3–C_5 hydrocarbons from cracking), S_{others} (C_7–C_8 hydrocarbons), S_{dimers} (C_9–C_{12} dimers), $S_{trimers}$ (C_{13}–C_{18} trimers), and S_{heavy} (C_{19}–C_{30} heavy oligomers).

3. Results and discussion

3.1. Characterization of M-SBA-15 materials

3.1.1. Al-SBA-15

The samples were named as Al-SBA-15 (*X*) where *X* varies depending on the Si/Al molar ratio used in the synthesis (*X* = 1 for Si/Al = 60, *X* = 2 for Si/Al = 30 and *X* = 3 for Si/Al = 10). The main physicochemical properties of the calcined Al-SBA-15 samples are summarized in Table 1. The final Si/Al atomic ratio in the calcined Al-SBA-15 samples is similar to those loaded in the synthesis medium, except for the highest Si/Al atomic ratio (Si/Al = 60) for

Table 1
Physicochemical properties of the calcined Al-SBA-15 materials.

Material	$(Si/Al)_{synthesis}$	$(Si/Al)^a_{final}$	$(Al^{IV}/Al^{VI})^b$	BET area (m^2 g^{-1})	Pore volume (cm^3 g^{-1})	Pore size (nm)[c]	d_{100} (nm)	Wall thickness (nm)[d]
SBA-15	∞	∞	–	651	0.96	8.0	10.2	3.8
Al-SBA-15 (1)	60	86	2.6	784	1.32	11.4	10.8	1.1
Al-SBA-15 (2)	30	30	1.9	788	1.34	12.0	11.3	1.1
Al-SBA-15 (3)	10	12	1.8	607	1.27	12.7	12.0	1.2

[a] Determined by ICP analysis.
[b] Determined from ^{27}Al-MAS-NMR (area $\delta = 54$ ppm area^{-1} $\delta = 0$ ppm).
[c] Determined from the maximum of BJH pore size distribution.
[d] Wall thickness was calculated as: a_0—pore size ($a_0 = 2 \times d_{100}/\sqrt{3}$).

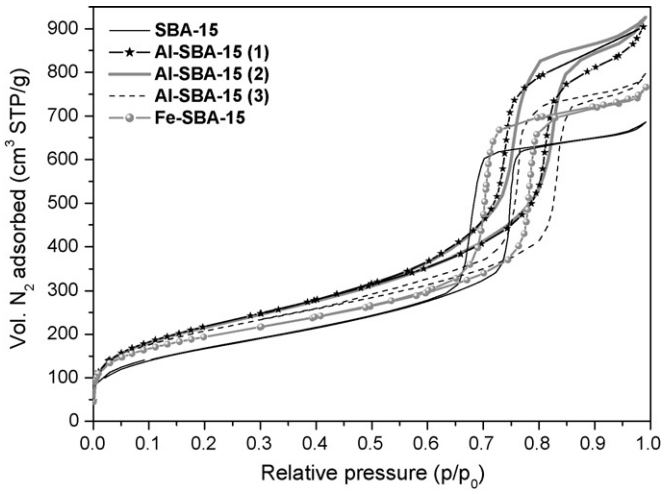

Fig. 2. N_2 adsorption–desorption isotherms of Al-SBA-15, Fe-SBA-15 and pure-siliceous SBA-15 materials.

which the final Si/Al is meaningfully higher (Si/Al = 86). XRD patterns of the calcined Al-SBA-15 samples are shown in Fig. 1. An additional XRD pattern of a pure siliceous SBA-15 is also included for comparison purposes. Al-SBA-15 samples present three well-resolved diffraction peaks, with a main peak at $2\theta \sim 0.9^\circ$ and two smaller ones placed around $2\theta \sim 1.4$ and 1.6°, respectively. They can be indexed as the (1 0 0), (1 1 0) and (2 0 0) *h k l* reflections associated with P6 mm hexagonal symmetry typical of SBA-15 materials [35]. As inferred from Table 1 data, the *d*-spacing of the (1 0 0) plane is shifted to higher values with increasing aluminium content, changing from 10.2 nm for siliceous SBA-15 to 12.0 for Al-SBA-15 (3) sample. Similar results have been previously observed [36] and they seem to be related with the longer Al–O bond length compared to the Si–O bond [37,38].

Nitrogen adsorption–desorption isotherms at 77 K of the three Al-SBA-15 samples are shown in Fig. 2. They correspond to the type IV of IUPAC classification, assigned to mesoporous materials, and exhibit a clear H1-type hysteresis loop at high relative pressure values, typical for SBA-15 mesoporous materials [27,35]. Table 1 summarizes the textural properties of these materials compared to those of SBA-15 supports. As observed, pore volumes increased in Al-SBA-15 samples ($\sim$1.3 $cm^3\ g^{-1}$) with regard to siliceous SBA-15 ($\sim$1.0 $cm^3\ g^{-1}$). In addition, the pore size increases steadily upon insertion of aluminium (from 8.0 to 12.7 nm), in agreement with the literature [36,39,40]. Larger pores detected in Al-SBA-15 materials are responsible for the lower wall thickness values as shown in Table 1, diminishing from around 3.8 nm of siliceous SBA-15 to roughly 1.2 for every Al-SBA-15 samples. These results suggest lower hydrothermal stability of aluminium-containing SBA-15 materials than that corresponding to the pure siliceous sample, probably related to the lower acidity used for preparing Al-SBA-15 solids (pH 1.5 for Al-SBA-15 and pH < 0 for siliceous SBA-15).

Table 1 includes the ratio tetrahedral/octahedral aluminium of the three samples determined from ^{27}Al-MAS-NMR spectra by division of the peak area detected at 54 ppm (assigned to tetrahedral aluminium) to the peak area at 0 ppm (associated with octahedral aluminium). The three Al-SBA-15 samples exhibit more tetrahedral aluminium centres than octahedral ones and it seems that the ratio tetrahedral/octahedral diminished with increasing aluminium contents.

3.1.2. Fe-SBA-15

Fe-SBA-15 sample was prepared following the method described by Martinez et al. [32] with a starting Si/Fe ratio of 30. ICP analysis determined a final Si/Fe ratio of 47 thus, the degree of iron incorporation achieved was 64%. Fig. 1 also exhibits the XRD pattern of the Fe-SBA-15 sample compared with a pure siliceous SBA-15. Fe-SBA-15 shows the main reflections of SBA-15 materials corresponding to (1 0 0), (1 1 0) and (2 0 0) planes. The d_{100} spacing of Fe-SBA-15 was 9.7 nm, close to that of siliceous SBA-15. Then, the incorporation of iron (at least to the extent reported by this method) did not disrupt the mesoscopic hexagonal ordering classical of SBA-15. Fig. 2 also depicts the nitrogen adsorption isotherm at 77 K of the Fe-SBA-15 sample together with that of pure-siliceous SBA-15. They are rather similar, and correspond to a type IV of IUPAC classification with a H1 hysteresis loop. The textural properties obtained from this Fe-SBA-15 (BET surface area = 682 $m^2\ g^{-1}$, pore volume = 1.15 $cm^3\ g^{-1}$, pore size = 9.4 nm and wall thickness = 1.7 nm) show values according to the expected ones for a standard SBA-15 material.

3.1.3. B-SBA-15

Two different direct synthesis methods (hydrothermal and sol–gel) were developed for the preparation of B-SBA-15. Three boron sources were tested with our hydrothermal and sol–gel methods: solid boric acid, aqueous boric acid and boron isopropoxide. The obtained samples with the hydrothermal method were denoted as B-SBA-15-hd (*X*) while those of the sol–gel method were named as B-SBA-15-sg (*X*) where *X* varies depending on the boron source (1 = solid boric acid, 2 = aqueous boric acid, 3 = boron isopropoxide). All the syntheses were carried out using a starting Si/B atomic ratio of 30. Table 2 shows the final Si/B present in the obtained B-SBA-15 materials. Solid boric acid was the boron source that led towards the highest degree of boron incorporation into the SBA-15 framework with both hydrothermal and sol–gel methods. Thus, Si/B atomic ratios of 51 and 65 were attained with sol–gel and hydrothermal method, respectively. Consequently, for the same boron source, sol–gel procedure allowed higher degree of boron incorporation than hydrothermal method. This feature is clearly shown with the other two boron sources, aqueous boric acid and boron isopropoxide. This fact suggests that the incorporation of boron species via condensation with the silica units is favoured at no strongly acid pH in the synthesis gel, since in sol–gel method pH is raised up to 4.

Fig. 3 illustrates the XRD patterns of calcined B-SBA-15-hd (1), B-SBA-15-sg (1) and pure-siliceous SBA-15, the latter included for

Table 2
Physicochemical properties of B-SBA-15 materials.

Material	$(Si/B)_{synthesis}$	$(Si/B)^a_{final}$	BET area ($m^2\ g^{-1}$)	Pore volume ($cm^3\ g^{-1}$)	Pore size (nm)[b]
SBA-15	∞	∞	651	0.96	8.0
B-SBA-15-hd (1)	30	65	680	0.97	6.5
B-SBA-15–hd (2)	30	103	695	1.10	7.2
B-SBA-15-hd (3)	30	105	701	1.10	7.5
B-SBA-15-sg (1)	30	51	686	0.85	5.2
B-SBA-15-sg (2)	30	62	697	0.94	6.3
B-SBA-15-sg (3)	30	74	700	1.08	7.1

[a] Determined by ICP analysis.
[b] Determined from the maximum of BJH pore size distribution.

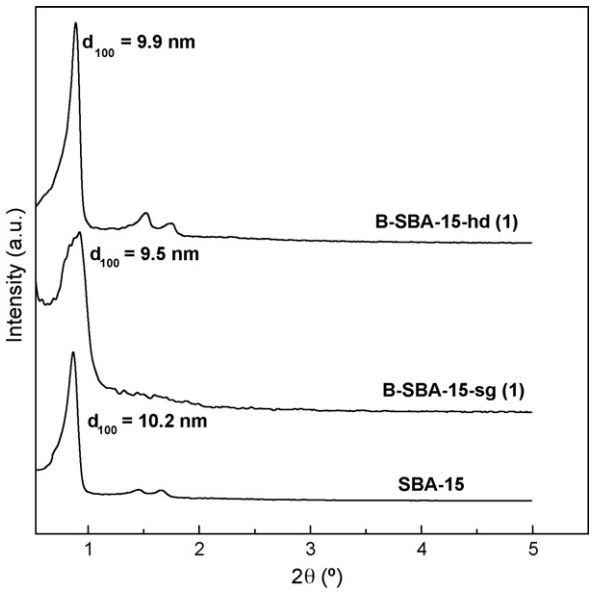

Fig. 3. XRD patterns of calcined B-SBA-15-hd (1), B-SBA-15-sg (1) and SBA-15 materials.

comparison. B-SBA-15-hd (1) exhibits the three reflections characteristic of SBA-15, indicating that the boron incorporation by the hydrothermal method leads to the mesoscopic ordering of the SBA-15 framework. In addition, the d_{100} spacing (9.9 nm) is somewhat lower to that of pure-silica SBA-15 (10.2 nm). This fact is in agreement with the lower size of boron compared to silicon and the consequent shortening of the M–O distance. XRD pattern of calcined B-SBA-15-sg (1) showed only the main reflection of the (1 0 0) plane with displacement towards lower values (d_{100} = 9.5 nm). The absence of the (1 1 0) and (2 0 0) peaks as well as the less intense and broader feature of the (1 0 0) reflection for this sample indicate a lower degree of mesoscopic hexagonal ordering. These results are in agreement with those previously reported by Aguado et al. [41] focused on the aluminium incorporation into MCM-41 structure by a very similar synthesis procedure. Thus sol–gel method makes easier the incorporation of heteroatoms into a siliceous structure but disturb the hexagonal ordering of the pores leading to a wormhole-like material. This fact can be confirmed by means of transmission electron microscopy. Fig. 4(a) and (b) shows TEM micrographs of B-SBA-15-hd (1) and B-SBA-15-sg (1), respectively. As observed, B-SBA-15-hd (1) exhibits a well-organized hexagonal mesoporous structure whereas B-SBA-15-sg (1) presents a wormhole-like arrangement indicating a less degree of mesoporous ordering.

Fig. 5 illustrates the nitrogen adsorption isotherms at 77 K of the three samples, B-SBA-15-hd (1), B-SBA-15-sg (1) and pure-siliceous SBA-15, the latter included for comparison. The three isotherms exhibit the shape of type IV of IUPAC classification, typical of mesoporous materials. However, some differences can be envisaged. The isotherms of both B-SBA-15-hd (1) and SBA-15 are very similar with a steep jump at P/P_0 = 0.6–0.7 from capillary condensation into the mesopores. In contrast, the corresponding jump for B-SBA-15-sg (1) is fairly less marked giving rise to lower pore volumes. Table 2 summarizes the main textural properties of the obtained B-SBA-15 materials. All of them give rise to similar BET surface areas (680–700 $m^2\,g^{-1}$), regardless of the synthesis procedure. In contrast, pore volumes of B-SBA-15-sg samples are distinctly lower than the equivalent B-SBA-15-hd ones. Likewise, pore sizes of B-SBA-15-sg are smaller than those of the equivalent B-SBA-15-hd

In order to study the boron coordination in the silica framework, ^{11}B MAS-NMR spectrum of B-SBA-15-sg (1) calcined sample is illus-

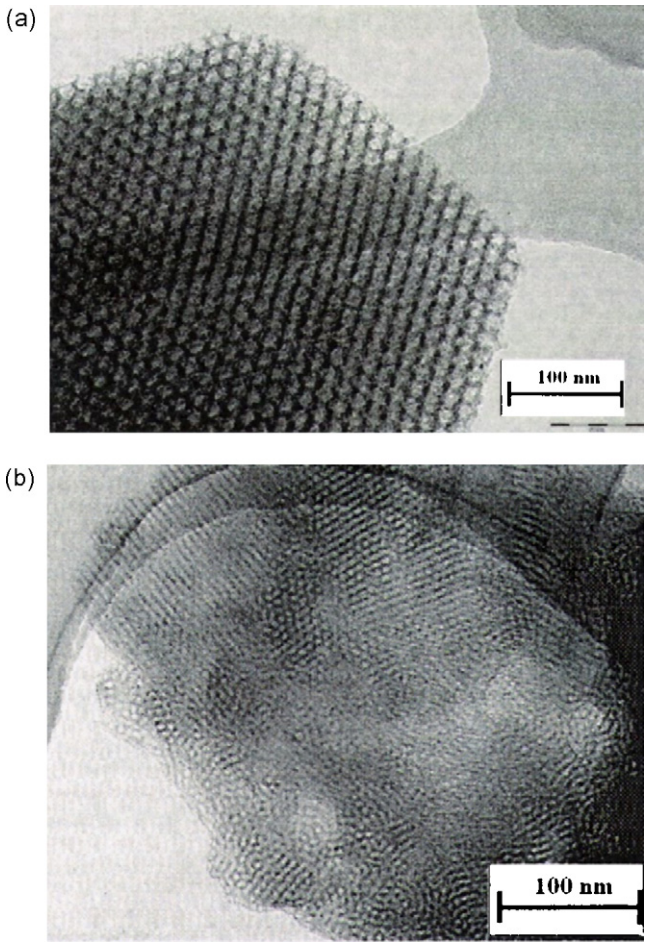

Fig. 4. TEM micrographs of B-SBA-15-hd (1) and B-SBA-15-sg (1) samples.

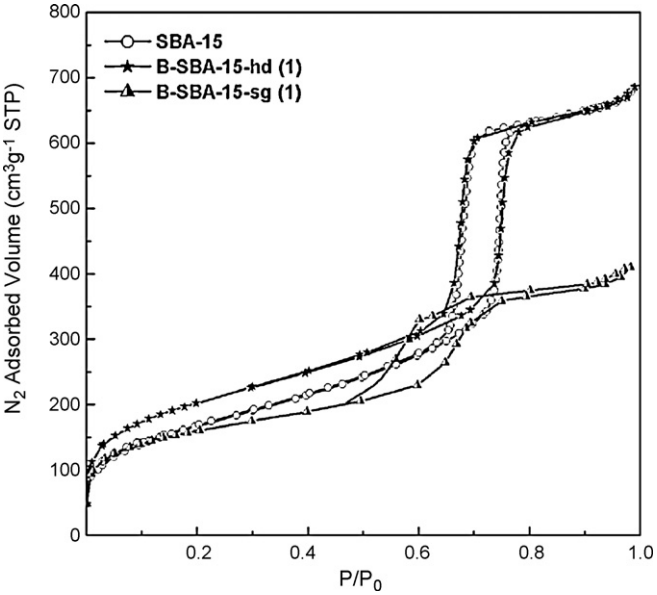

Fig. 5. N_2 adsorption isotherms at 77 K of calcined B-SBA-15-hd (1), B-SBA-15-sg (1) and SBA-15 materials.

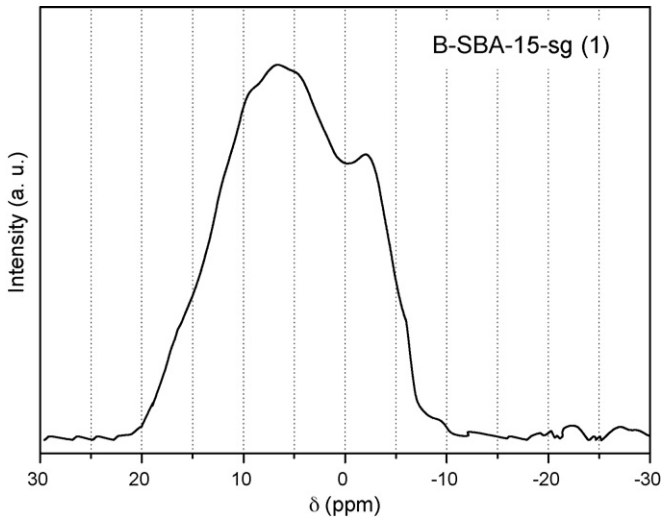

Fig. 6. ^{11}B MAS–NMR for B-SBA-15-sg (1) sample.

trated in Fig. 6 (this material presents the highest boron content). As it is reported in the literature [42–44], two signals at 8–9 ppm and −2.2 ppm showed up. The small peak centered at −2.2 ppm is associated to boron in tetrahedral coordination within the framework. However, the broad signal around 8 ppm, typical for trigonal boron species, suggests that this kind of boron remains in the framework after the calcination of the material and seems to be the main boron specie. Trigonal boron sites are formed by dehydratation from the tetrahedral boron sites mainly present in the "as-made" material. According to the literature [42–45], only tetrahedral boron sites are considered as acid centres. Therefore, since the B-SBA-15 framework is mainly constituted by trigonal boron sites, a very low acidity is expected for these materials.

3.1.4. Cr-SBA-15

The samples were denoted as Cr-SBA-15 (*X*), where *X* varies depending on the synthesis pH (*X* = 1 for pH 1.5, *X* = 2 for pH 3 and *X* = 3 for pH 5). Table 3 summarizes the physicochemical properties of the calcined Cr-SBA-15 materials. Although the starting Si/Cr atomic ratio in all the syntheses was 30, the final Si/Cr atomic ratios were very low, at best 240 for pH 5. In addition, the Si/Cr atomic ratio decreased with the pH, diminishing from >1000 for pH 1.5–240 at pH 5. Then, the method allows a low incorporation degree of chromium even at pH 5. These results of chromium incorporation are much lower than those obtained by Aguado et al. [27] in the direct synthesis of chromium and aluminium-containing SBA-15 materials by the same hydrothermal procedure. This fact could be ascribed to the increase in structural faults induced by the presence of aluminium into the silica network, making easier the incorporation of another heteroatom from the synthesis gel.

XRD patterns of calcined Cr-SBA-15 materials are shown in Fig. 7. All the samples show the three reflections of (1 0 0), (1 1 0) and (2 0 0) *h k l* planes typical of SBA-15 materials corresponding to the hexagonal mesoscopic ordering for Cr-SBA-15 samples. In addition, their *d*-spacings are rather similar and around 10.0 (see Table 3). This high degree of ordering is remarkable considering the high pH values used during the synthesis (pH 1.5, 3 and 5). According to works previously reported [27,46], working at pH > 2 (silica isoelectric point) the assembly of the mesostructure can occur by means of hydrogen bonds formation between neutral silica and surfactant (S^0I^0). This mechanism allows the typical SBA-15 structure in non-strongly acid medium to be obtained and, in this case, increases slightly the incorporation of the heteroatom.

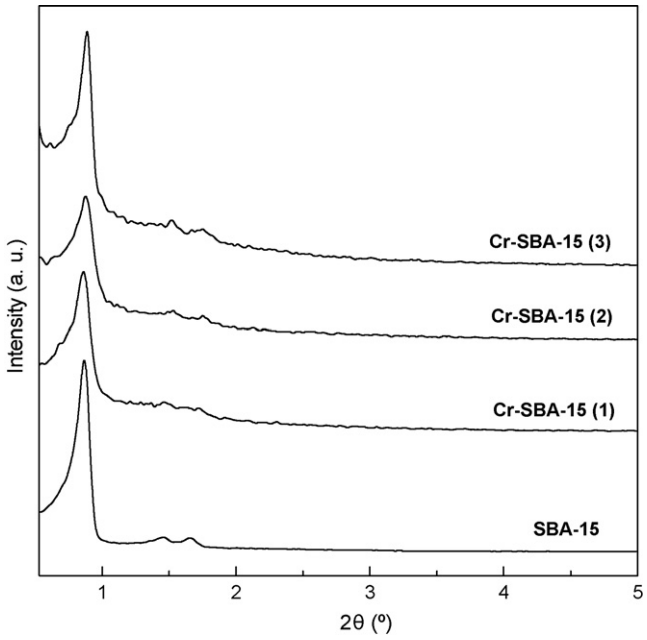

Fig. 7. XRD patterns of calcined Cr-SBA-15 materials.

Textural properties of calcined Cr-SBA-15 materials are summarized in Table 3. Pore volumes were fairly similar to the corresponding one of siliceous SBA-15 (0.9–1.1. $cm^3\ g^{-1}$). In contrast, BET surface areas of Cr-SBA-15 and pore sizes are meaningfully higher than that of siliceous SBA-15. Consequently, the incorporation of Cr leads to a lower pore wall thickness (1.5–2.0) despite the low amount of Cr incorporated. This fact agrees with the previously reported results obtained with aluminium in Al-SBA-15 and it is probably related to the lower acidity used during Cr-SBA-15 synthesis regarding to pH < 0 used for siliceous SBA-15.

Calcined Cr-SBA-15 samples were characterized by UV–vis spectroscopy in order to determine the kind of Cr species existing in these materials after calcination. Fig. 8 shows the Cr-SBA-15 (2) and Cr-SBA-15 (3) UV–vis spectra. It can be observed that both catalysts present three signals centred around 240, 360 and 450 nm which are assigned to the $O \rightarrow Cr^{6+}$ charge transfer transitions of chromate and dichromate [47,48]. The absence of chromium (III) oxide band at 560 nm indicates a total oxidation of Cr^{3+} (chromium precursor is trivalent) to Cr^{6+} during the calcination step.

Table 3
Physicochemical properties of Cr-SBA-15 materials.

Material	pH	$(Si/Cr)_{synthesis}$	$(Si/Cr)^a_{final}$	BET area ($m^2\ g^{-1}$)	Pore volume ($cm^3\ g^{-1}$)	Pore size (nm)[b]	d_{100} (nm)	Wall thickness (nm)[c]
SBA-15	–	∞	∞	651	0.96	8.0	10.2	3.8
Cr-SBA-15 (1)	1.5	30	>1000	902	1.13	10.4	10.2	1.4
Cr-SBA-15 (2)	3	30	360	819	0.92	9.6	9.9	2.0
Cr-SBA-15 (3)	5	30	240	731	0.89	9.6	10.6	1.8

[a] Determined by ICP analysis.
[b] Determined from the maximum of BJH pore size distribution.
[c] Wall thickness were calculated as: a_0—pore size ($a_0 = 2 \times d_{100}/\sqrt{3}$).

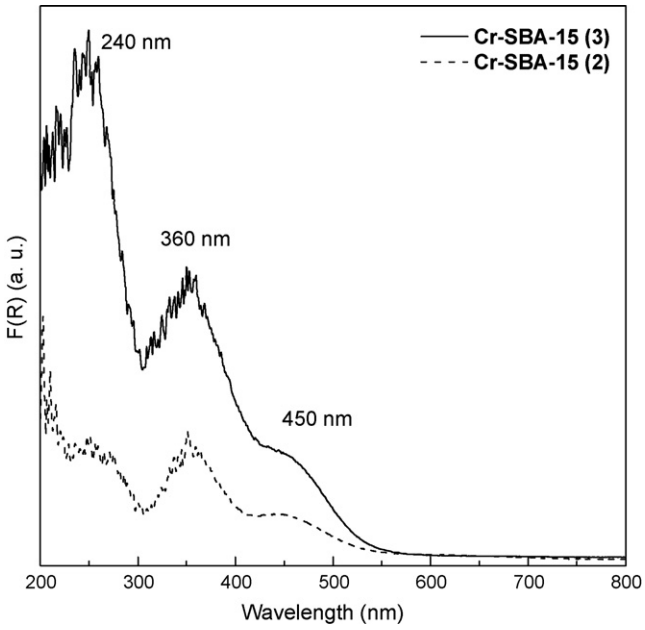

Fig. 8. UV–vis spectra of calcined Cr-SBA-15 (2) and Cr-SBA-15 (3) materials.

3.2. Catalysts acidity and results in 1-hexene oligomerization

The oligomerization reactions of 1-hexene usually proceed by means of an acid catalysed mechanism comprising the following set of reactions (among similar others) [16]:

Oligomerization : $C_6^= \rightarrow C_{12}^= \rightarrow C_{18}^= \rightarrow C_{24}^= \rightarrow$ etc.

Cracking : $C_{12}^= \rightarrow C_4^= + C_8^=$

Alkylation : $C_4^= + C_6^= \rightarrow C_{10}^=$

These reactions are usually accompanied by double bond shift (fast), skeletal isomerization and hydrogen transfer. The latter are responsible for the formation of saturates, alkanes, polyenes and aromatics, which are coke precursors. These reactions are meant to occur to an extent that depends on the physicochemical properties of every acid site.

The acid properties of the materials were determined by means of ammonia TPD measurements. Table 4 summarizes the acid properties of the calcined Al-SBA-15, Fe-SBA-15 and Cr-SBA-15 materials. All the Al-SBA-15 samples showed a similar acid strength distribution since the temperature of the maximum of ammonia desorption was placed around 260 °C, regardless of the aluminium content. The content of acid sites increased with the aluminium amount in the catalysts from 0.1 meq NH_3 g^{-1} for Al-SBA-15 (1) (Si/Al = 86) to 0.56 meq NH_3 g^{-1} for Al-SBA-15 (3) (Si/Al = 12). Fe-SBA-15 exhibited also a medium acid strength distribution with a maximum of ammonia desorption placed at 259 °C and a number of acid sites between values corresponding to Al-SBA-15 (1) and Al-SBA-15 (2), in agreement with the heteroatom content. Therefore the incorporation of iron into SBA-15 structure leads to similar acid sites distribution than that achieved by the introduction of aluminium. Cr-SBA-15 samples show a low content of acid sites (0.05–0.08 meq NH_3 g^{-1}) due to their very low chromium contents (Si/Cr—240–360) but the acid strength of these materials is higher than that observed for aluminium and iron-containing SBA-15 materials. These results are in agreement with some works previously reported which have showed that the incorporation of chromium species on mesoporous materials leads medium and strong acid sites [49,50]. Acidity values obtained for B-SBA-15 samples by means of NH_3-TPD experiments were almost negligible and for this reason are not shown in Table 4. The poor acidity associated with boron trigonal species detected by ^{11}B MAS NMR is behind these results.

Table 4
Acid properties of the calcined M-SBA-15 catalysts.

Catalyst	Heteroatom	Si/M molar ratio	T_{max} (°C)[a]	Acidity (meq NH_3 g^{-1})[a]
Al-SBA-15 (1)	Al	86	262	0.10
Al-SBA-15 (2)	Al	30	259	0.21
Al-SBA-15 (3)	Al	12	260	0.56
Fe-SBA-15	Fe	47	259	0.13
B-SBA-15-hd (1)	B	65	–	–
B-SBA-15-sg (1)	B	51	–	–
Cr-SBA-15 (2)	Cr	360	304	0.05
Cr-SBA-15 (3)	Cr	240	315	0.08

[a] Calculated from ammonia TPD measurements.

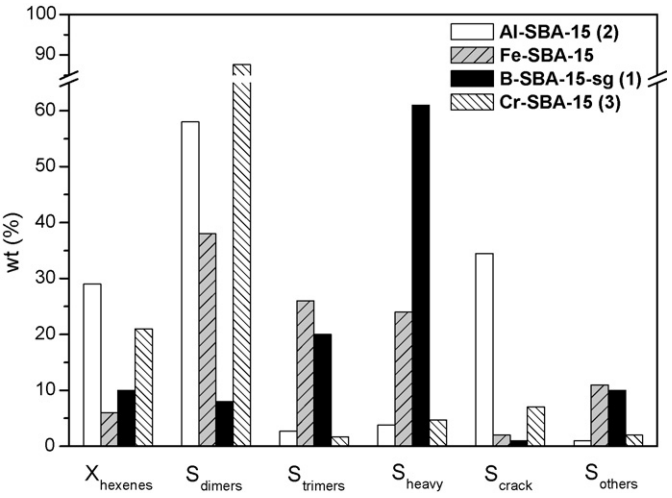

Fig. 9. 1-Hexene oligomerization over M-SBA-15 materials.

Fig. 9 illustrates the results obtained in the oligomerization of 1-hexene at 125 °C over some selected catalysts: Al-SBA-15 (2), Fe-SBA-15, B-SBA-15-sg (1) and Cr-SBA-15 (3). The conversion was always below 30%, regardless of the tested catalyst, likely due to the low reaction temperature (125 °C) [51]. As expected, the highest conversion was obtained with the most acid catalyst (Al-SBA-15 (2)). As well, it is remarkable the high conversion observed for Cr-SBA-15 sample despite its very low heteroatom content (Si/Cr = 240). This result could be related to the higher acid strength of chromium centres detected by ammonia TPD since stronger acidity leads to higher activity in this kind of reactions [52]. On the other hand, Fe-SBA-15 catalyst showed an intermediate acidity value (0.13 meq NH_3 g^{-1}), but its activity in the oligomerization of 1-hexene is lower than that observed for less acid samples (Cr-SBA-15 and B-SBA-15-sg (1)). Different factors must be considered in order to support these results. First, nature of acid centres detected for Fe-SBA-15 and Cr-SBA-15 materials is different and thus their catalytic behaviour is also different. Specifically, chromium centres are more active than iron centres. By comparing Fe-SBA-15 and B-SBA-15-sg (1) catalysts, it must be considered that the first one was prepared by a hydrothermal method whereas the second one was synthesized by a sol–gel method. Therefore, mesoscopic order of both structures is significantly different: sol–gel procedure leads to wormhole-like structures whereas hydrothermal materials show a perfect hexagonal symmetry. It is possible that wormhole-like structure makes easier the access of molecules on active centres increasing the catalytic activity. Thus, B-SBA-15-sg (1) is more active

than Fe-SBA-15 despite its negligible acidity. In this sense, previous works have showed that mesoporous materials with lower ordering are more active in different reactions than materials with a high hexagonal symmetry [53]. In conclusion, regarding the ratio conversion/heteroatom content, the following heteroatom performance can be deduced: Cr > Al > B > Fe.

Regarding to the selectivity, since 1-hexene conversion is considerably different depending on the catalyst tested, it is difficult to conclude from the comparison among the different samples. However, the trend showed for each catalyst to produce different kinds of products can be properly evaluated. So, Al-SBA-15 (2) and Cr-SBA-15 (3) samples generate much more dimers than trimers and heavy oligomers probably due to its higher or stronger acidity, respectively. Thus, for these two catalysts $S_{dimers} \gg S_{trimers} + S_{heavy}$. Fe-SBA-15 catalyst produces a similar amount of dimers than trimers and heavy oligomers ($S_{dimers} \sim S_{trimers} + S_{heavy}$), indicating a greater extension of the oligomerization reaction. However, most promising selectivity trend was observed for B-SBA-15-sg (1) catalyst obtaining a very high selectivity towards heavy oligomers, a considerable production of trimers and less than 10% of dimers. So, $S_{heavy} \gg S_{trimers} + S_{dimers}$ being this selectivity trend totally opposite than that previously described for the others heteroatoms. In this case, it seems that heavy oligomers and trimers are formed as primary products and not as secondary ones from oligomerization of the dimmers fraction. A hypothetical explanation of this behaviour could be that the dimeric carbocation, once formed over the boron acid site, undergoes skeletal isomerization, hydride shift and oligomerization towards heavy oligomers before eliminating a proton. Thereby, the formation of the more stable trimer and heavy carbocations takes place. This mechanism is similar to the one that explains the formation of preferentially trimers in the oligomerization of propene over solid phosphoric acid [2]. In this regard, boron acid site shows a completely different performance to the aluminium site. Therefore, B-SBA-15-sg (1) material shows the most promising products distribution for being used in the formulation of gasoline or diesel by means of 1-hexene oligomerization processes. In this sense, optimization of the synthesis procedure to improve boron incorporation into silica framework and/or changes of boron coordination in order to yield a more acid content would be interesting alternatives to explore for increasing the catalytic activity of these boron-containing materials.

4. Conclusions

Different M-SBA-15 materials (M = Al, B, Cr, Fe) have been prepared by direct synthesis methods. Al-SBA-15 samples were synthesized with Si/Al = 12–86 using aluminium isopropoxide as aluminium source. The increase in aluminium content led towards a more disordered mesoporous framework. B-SBA-15 was synthesized using two direct synthesis methods: sol–gel and hydrothermal and three different boron sources: solid boric acid, aqueous boric acid and boron isopropoxide. The highest degree of boron incorporation was achieved with solid boric acid for both methods (51–65). The sol–gel procedure gave rise to the formation of a more distorted mesoporous framework with the higher boron content while the hydrothermal led towards a material with higher mesoscopic ordering. ^{11}B MAS NMR spectra of B-SBA-15sg (1) showed that trigonal boron is the principal boron coordination state in the SBA-15 framework obtained after calcination, not associated to acid sites. Cr-SBA-15 was also prepared by direct synthesis method at different pH (1.5, 3, 5). The chromium incorporation degree increased with the pH but it was low, at best Si/Cr = 240 at pH 5. Despite the pH increase, Cr-SBA-15 materials showed good mesoscopic ordering. According to UV measurements, chromium species formed after calcination were Cr(VI) for all the catalysts.

Oligomerization of 1-hexene at 125 °C over the different M-SBA-15 materials indicated that the highest conversion was attained over Al-SBA-15 (2) due to the high acidity of this material. On the other hand, Cr-SBA-15 materials exhibited high conversion despite its low heteroatom content (Si/Cr = 240). This result is probably due to the higher acid strength of chromium centres detected by ammonia TPD. Fe-SBA-15 catalyst showed an intermediate acidity but its activity in the oligomerization of 1-hexene is lower than that observed for less acid samples (Cr-SBA-15 and B-SBA-15-sg (1)). Different nature of acid centres detected for Fe-SBA-15 and Cr-SBA-15 materials and differences of mesoscopic ordering observed for Fe-SBA-15 and B-SBA-15-sg (1) structures led to these results.

Regarding to the selectivity towards oligomerization products, different trends were observed by changing the heteroatom. So, Al-SBA-15 (2) and Cr-SBA-15 (3) samples generate much more dimers than trimers and heavy oligomers ($S_{dimers} \gg S_{trimers} + S_{heavy}$). Fe-SBA-15 catalyst produces a similar amount of dimers than trimers and heavy oligomers ($S_{dimers} \sim S_{trimers} + S_{heavy}$), whereas most promising selectivity trend was observed for B-SBA-15-sg (1) catalyst obtaining a very high selectivity towards heavy oligomers, a considerable production of trimers and less than 10% of dimers ($S_{heavy} \gg S_{trimers} + S_{dimers}$). Therefore, B-SBA-15-sg (1) material shows a promising products distribution for being used in the formulation of gasoline or diesel by means of 1-hexene oligomerization processes.

References

[1] G. Ertl, H. Knözinger, J. Weitkamp, Handbook of Heterogeneous Catalysis, Wiley VCH, Weinheim, 1997, p. 2380.
[2] G.A. Olah, A. Molnar, Hydrocarbon Chemistry, John Wiley & Sons Inc., New York, 1995, p. 524.
[3] R.J. Quann, L.A. Green, S.A. Tabak, F.J. Krambeck, Chemistry of olefin oligomerization over ZSM-5 catalyst, Ind. Eng. Chem. Res. 27 (1988) 565–570.
[4] G.F. Froment, J. De Meyer, E.G. Derouane, Deactivation of zeolite catalysts by coke formation, J. Catal. 124 (1990) 391–400.
[5] S.A. Tabak, F.J. Krambeck, W.E. Garwood, Conversion of propylene and butylene over ZSM-5 catalyst, AICHE 32 (1986) 1526–1531.
[6] H. van Bekkum, E.M. Flanigen, Introduction to Zeolite Science and Practice, Elsevier, Amsterdam, 2001, p. 1062.
[7] C.S.H. Chen, R.F. Bridger, Shape-selective oligomerization of alkenes to near-linear hydrocarbons by zeolite catalysis, J. Catal. 161 (1996) 687–693.
[8] J.P.G. Pater, P.A. Jacobs, J.A. Martens, 1-hexene oligomerization in liquid, vapor, and supercritical phases over beidellite and ultrastable Y zeolite catalysts, J. Catal. 179 (1998) 477–482.
[9] J.E. Stanat, G.M.K. Mathys, D.W. Turner, J.C. Cheng, S.W. Beadle, C.M. Cheng-Guajardo, R.R. Eijkhoudt, A.D. Godwin, E.E. Green, C.M. Yarbrough, R.F. Caers, C.B. Duncan, R.Y. Saleh, WO Patent 2003082780 A1 (2003).
[10] A. Giusti, S. Gusi, G. Bellusi, V. Fattore, Eur. Pat. Appl. EP Patent 290068 A1 (1998).
[11] J.A. Martens, R. Ravishankar, I.E. Mishin, P.A. Jacobs, Tailored alkene oligomerization with H-ZSM-57 zeolite, Angew. Chem. Int. Ed. 39 (2000) 4376–4379.
[12] H. Abrevaya, R. Frame, US Patent 6403853 B1 (2002).
[13] S. Peratello, C. Perego, G. Bellusi, US Patent 5342814 (1994).
[14] J.P.G. Pater, P.A. Jacobs, J.A. Martens, Oligomerization of hex-1-ene over acidic aluminosilicate zeolites, MCM-41, and silica-alumina co-gel catalysts: a comparative study, J. Catal. 184 (1999) 262–267.
[15] M. Yamamura, K. Chaki, T. Wakatsuki, H. Okado, K. Fujimoto, Synthesis of ZSM-5 zeolite with small crystal size and its catalytic performance for ethylene oligomerization, Zeolites 14 (1994) 643–649.
[16] R. Van Grieken, J.M. Escola, J. Moreno, R. Rodriguez, Liquid phase oligomerization of 1-hexene over different mesoporous aluminosilicates (Al-MTS, Al-MCM-41 and Al-SBA-15) and micrometer/nanometer HZSM-5 zeolites, Appl. Catal. A 305 (2006) 176–188.
[17] B. Chiche, E. Sauvage, F. Di Renzo, I.I. Ivanova, F. Fajula, Butene oligomerization over mesoporous MTS-type aluminosilicates, J. Mol. Catal. A: Chem. 134 (1998) 145–157.
[18] V. Hulea, F. Fajula, Ni-exchanged AlMCM-41—an efficient bifunctional catalyst for ethylene oligomerization, J. Catal. 225 (2004) 213–222.
[19] R. Catani, M. Mandreoli, S.S. Rosini, A. Vaccari, Mesoporous catalysts for the synthesis of clean diesel fuels by oligomerisation of olefins, Catal. Today 75 (2002) 125–131.
[20] R. Van Grieken, J.M. Escola, J. Moreno, R. Rodriguez, Nitrogen and sulphur poisoning in alkene oligomerization over mesostructured aluminosilicates (Al-MTS, Al-MCM-41) and nanocrystalline n-HZM-5, Appl. Catal. A 337 (2008) 173–183.

[21] A. de Klerk, Oligomerization of 1-hexene and 1-octene over solid acid catalysts, Ind. Eng. Chem. Res. 44 (2005) 3887–3893.
[22] I. Ferino, R. Monaci, V. Solinas, L. Forni, A. Rivoldini, L. Sanseverino, Transformation of 1-butene over synthetic zeolites, Collect. Czech. Chem. Commun. 57 (1992) 869–881.
[23] S. Wu, Y. Han, Y.-C. Zou, J.-W. Song, L. Zhao, Y. Din, S.-Z. Liu, F.-S. Xiao, Synthesis of heteroatom substituted SBA-15 by the "pH-adjusting" method, Chem. Mater. 16 (2004) 486–492.
[24] Y. Yue, A. Gédéon, J.-L. Bonardet, N. Melosh, J.-B. D'Espinose, J. Fraissard, Direct synthesis of AlSBA mesoporous molecular sieves: characterization and catalytic activities, Chem. Commun. 19 (1999) 1967–1968.
[25] B. Dragoi, E. Dumitriu, C. Guimon, A. Auroux, Acidic and adsorptive properties of SBA-15 modified by aluminum incorporation, Microporous Mesoporous Mater. 121 (2009) 7–17.
[26] J. Wang, Q. Liu, A simple method to directly synthesize Al-SBA-15 mesoporous materials with different Al contents, Solid State Commun. 148 (2008) 529–533.
[27] J. Aguado, G. Calleja, A. Carrero, J. Moreno, One-step synthesis of chromium and aluminium containing SBA-15 materials—new phillips catalysts for ethylene polymerization, Chem. Eng. J. 137 (2008) 443–452.
[28] M. Selvaraj, S. Kawi, Direct synthesis of mesoporous CrSBA-15 catalyst and its high activity and selectivity for oxidation of anthracene, Mircroporous Mesoporous Mater. 101 (2007) 240–249.
[29] M. Selvaraj, S. Kawi, D.-W. Park, C.-S. Ha, Synthesis and characterization of GaSBA-15: effects of synthesis parameters and hydrothermal stability, Microporous Mesoporous Mater. 117 (2009) 586–595.
[30] J.A. Melero, J.M. Arsuaga, P. de Frutos, J. Iglesias, J. Sainz, S. Blázquez, Direct synthesis of titanium-substituted mesostructured materials using non-ionic surfactants and titanocene dichloride, Microporous Mesoporous Mater. 1–3 (2005) 364–373.
[31] B.L. Newalkar, J. Olanrewaju, S. Komarneni, Microwave-hydrothermal synthesis and characterization of zirconium substituted SBA-15 mesoporous silica, J. Phys. Chem. B 105 (2001) 8356–8360.
[32] F. Martinez, Y.-J. Han, G. Stucky, J.L. Sotelo, G. Ovejero, J.A. Melero, Synthesis and characterisation of iron-containing SBA-15 mesoporous silica, Stud. Surf. Sci. Catal. 142 (2002) 1109–1116.
[33] A. Vinu, D.P. Sawant, K. Ariga, K.Z. Hossain, S.B. Halligudi, M. Hartmann, M. Nomura, Direct synthesis of well-ordered and unusually reactive FeSBA-15 mesoporous molecular sieves, Chem. Mater. 17 (2005) 5339–5345.
[34] Y. Li, W. Zhang, L. Zhang, Q. Yang, Z. Wei, Z. Feng, C. Li, Direct synthesis of Al-SBA-15 mesoporous materials via hydrolysis-controlled approach, J. Phys. Chem. B 108 (2004) 9739–9744.
[35] D. Zhao, J. Feng, Q. Huo, N. Melosh, G.H. Fredrickson, B.F. Chmelka, G.D. Stucky, Triblock copolymer syntheses of mesoporous silica with periodic 50 to 300 angstrom pores, Science 279 (1998) 548–552.
[36] G. Calleja, J. Aguado, A. Carrero, J. Moreno, Preparation, characterization and testing of Cr/AlSBA-15 ethylene polymerization catalysts, Appl. Catal. A: Gen. 316 (2007) 22–31.
[37] A.P. Legrand (Ed.), The Surface Properties of Silicas, John Wiley & Sons Ltd., 1997, p. 2.
[38] P.S. Sklad, P. Angelini, Extended electron-energy loss fine-structure analysis of amorphous Al_2O_3, J. Sevely., Philos. Mag. A 65 (1992) 1445–1461.
[39] Y.-H. Yue, A. Gédéon, J.-L. Bonardet, J.B. d'Espinose, N. Melosh, J. Fraissard, Direct incorporation of A1 in SBA mesoporous materials: characterization, stability and catalytic activity, Stud. Surf. Sci. Catal. 129 (2000) 209–218.
[40] M.-A. Springuel-Huet, J.-L. Bonardet, A. Gédéon, Y. Yue, V.N. Romannikov, J. Fraissard, Mechanical properties of mesoporous silicas and alumina-silicas MCM-41 and SBA-15 studied by N-2 adsorption and Xe-129 NMR, Microporous Mesoporous Mater. 44–45 (2001) 775–784.
[41] J. Aguado, D.P. Serrano, J.M. Escola, A sol-gel approach for the room temperature synthesis of Al-containing micelle-templated silica, Microporous Mesoporous Mater. 34 (2000) 43–54.
[42] I. Eswaramoorthi, A.K. Dalai, Synthesis, characterisation and catalytic performance of boron substituted SBA-15 molecular sieves, Microporous Mesoporous Mater. 93 (2006) 1–11.
[43] V. Sundaramurthy, I. Eswaramoorthi, N. Lingappan, The catalytic effect of boron substitution in MCM41-type molecular sieves, Can. J. Chem. 82 (2004) 631–640.
[44] S. Liu, H. He, Z. Luan, J. Klinowski, Solid-state NMR studies of the borosilicate mesoporous molecular sieve MCM-41, J. Chem. Soc. Faraday Trans. 92 (1996) 2011–2015.
[45] S.-J. Hwang, C.-Y. Chen, S.Y. Zones, Boron sites in borosilicate zeolites at various stages of hydration studied by solid state NMR spectroscopy, J. Phys. Chem. B. 108 (2004) 18535–18546.
[46] G.J.A.A. Soler-Illia, E.L. Crepaldi, D. Grosso, C. Sánchez, Block copolymer-templated mesoporous oxides, Curr. Opin. Colloid Interf. Sci. 8 (2003) 109–126.
[47] B.M. Weckhuysen, I.E. Wachs, R.A. Schoonheydt, Surface chemistry and spectroscopy of chromium in inorganic oxides, Chem. Rev. 96 (1996) 3327–3349.
[48] B.M. Weckhuysen, L.M. De Ridder, R.A. Schoonheydt, A quantitative diffuse reflectance spectroscopy study of supported chromium catalysts, J. Phys. Chem. 97 (1993) 4756–4763.
[49] E. Rombi, M.G. Cutrufello, V. Solinas, S. De Rossi, G. Ferraris, A. Pistone, Effects of potassium addition on the acidity and reducibility of chromia/alumina dehydrogenation catalysts, Appl. Catal. A 251 (2003) 255–266.
[50] S. Gómez, L.J. Garces, J. Villegas, R. Ghosh, O. Giraldo, S.L. Suib, Synthesis and characterization of TM-MCM-48 (TM = Mn, V, Cr) and their catalytic activity in the oxidation of styrene, J. Catal. 233 (2005) 60–67.
[51] J.M. Escola, R. Van Grieken, J. Moreno, R. Rodriguez, Liquid-phase oligomerization of 1-hexene using Al-MTS catalysts, Ind. Eng. Chem. Res. 45 (2006) 7409–7414.
[52] C. Flego, M. Marchionna, C. Perego, High quality diesel by olerin oligomerisation: new tailored catalysts, Stud. Surf. Sci. Catal. 158 (2005) 1271–1278.
[53] D.-W. Park, S.-D. Choi, S.-J. Choi, C.-Y. Lee, G.-J. Kim, Asymmetric epoxidation of styrene on the heterogenized chiral salen complexes prepared from organo-functionalized mesoporous materials, Catal. Lett. 78 (2002) 145–151.